Tomographic Reconstruction of a Three-Dimensional Flow Field with Limited Interferometric Data

Dong Jin Cha*

Key words : Three-dimensional flow fields, Flow diagnostics, Quantitative visualization, Holographic interferometric tomography, Ill-posed reconstruction

Abstract

Holographic interferometric tomography can provide reconstruction of instantaneous three-dimensional gross flow fields. The technique however confronts ill-posed reconstruction problems in practical applications. Experimental data are usually limited in projection and angular scanning when a field is captured instantaneously or under the obstruction of test models and test section enclosures. An algorithm, based on a series expansion method, has been developed to improve the reconstruction under the ill-posed conditions. A three-dimensional natural convection flow around two interacting isothermal cubes is experimentally investigated. The flow can provide a challenging reconstruction problem and lend itself to accurate numerical solution for comparison. The refractive index fields at two horizontal sections of the thermal plume with and without an opaque object are reconstructed at a limited view angle of 80° . The experimental reconstructions are then compared with those from numerical calculation and thermocouple thermometry. It confirms that the technique is applicable to reconstruction of reasonably complex, three-dimensional flow fields.

Nomenclature

A : Modulation amplitude function
a : Line integral transform of basis function
B : Background intensity function
b : Series expansion basis function
C : Coefficient of the corresponding basis function
g : Optical pathlength data, projection data
I : Intensity function
N : Number of basis functions
n : Refractive index field, object field

* Div. of Control and Instrumentation and Building Services Engineering, Taejon National University of Technology, Taejon, 305-320, Korea

p : Phase function
s : Probing ray
T : Temperature
x, y : Coordinates

Greek symbols

β : Volumetric coefficient of thermal expansion of a fluid
ε : Relative temperature difference
θ : Projection angle
λ : Laser wavelength
ρ : Distance from the optical axis

Subscripts

i, j : Index
∞ : Ambient

Superscripts

i, j : Index
NU : Numerical computation
RE : Tomographic reconstruction
TC : Thermocouple thermometry

1. Introduction

As the importance for more thermally efficient and enviromentally friendly facilities is emphasized, it requires to better understand complex, three-dimensional (3-D) flow fields in them, leading the needs for ever-sophistcating experimental techniques. Three-dimensional quantitative visualization techniques if feasible are very desirable for obtaining unprecedented physical insights of fluid flow phenomena. Currently, applications of planar gross-field techniques, including laser induced fluorescence and particle image velocimetry, are frequently employed in flow measurements, and at the same time those techniques are being under development for 3-D measurement capabilities. Also, holographic interferometric tomography (HIT), that is, reconstruction of 3-D refractive index fields from multidirectional projection holographic interferograms, can be a good candidate.

For simple cases of axisymmetric flow or flow without variation along probing rays, the use of holographic interferometer has already been a common practice in many applications. Even for general asymmetric fields, the HIT reconstructions have recently been reported by several investigators, typically in high-speed aerodynamics[1,2] and heat/mass transfer.[3,4] However, challenges in HIT arise in reliably reconstructing 3-D fields under adverse data collection environments that result in a limited data set. Refractive index fields to be measured by interferometry can be related to the physical properties of fluids such as density,[1] temperature,[3] chemical species concentrations,[5] etc.

HIT that consists of the three major steps of interferogram recording, data reduction, and computational tomographic reconstruction frequently encounters challenging problems of reconstructing fields under adverse data conditions. The flow field to be reconstructed by HIT gradually changes; however, it may encounter steep gradients at a boundary layer or discontinuity at a shock. In most cases, flow field interferometric data are also sparse and nonuniform in sampling and incomplete in projection and scanning. These problems arise when a field is captured instantaneously or under the presence of opaque test models and test section enclosures as demonstrated in Fig. 1. All of these adverse conditions result in ill-posed reconstruction.

In multidirectional interferometry, the optical pathlength data (OPD) $g(\rho, \theta)$ of a field section $n(x, y)$ perpendicular to projection interfero-

grams can be measured as a function of the projection angle θ and the distance ρ from the optical axis, as shown in Fig. 1. The projection data $g(\rho, \theta)$, which can be obtained over a view angle defined as the range of projection angles, is then the line integral of the refractive index field $n(x, y)$ to be reconstructed along a probing ray:

$$g(\rho, \theta) \cong \int_{ray} n(x, y) ds \tag{1}$$

Tomographic reconstruction of a flow field thus requires inversion of the line intergal transform. In this approach, 3-D field reconstruction can be accomplished by stacking up the reconstructed two-dimensional sections. Current reconstruction techniques[6] can be classified into two groups: transform methods[7] and series expansion methods.[8] Typical transform methods are those by the Fourier transform[9] and convolution backprojection.[10] Transform methods require uniform data points that are complete in projection and angular scanning, that is, unblocked projection and full view angle of 180°. In the practical applications, involving the use of insufficient data, they need to augment the data through interpolation. As the degree of ill-posedness increases, however, the interpolated data start to weigh more and become less accurate, thus distorting the reconstruction.

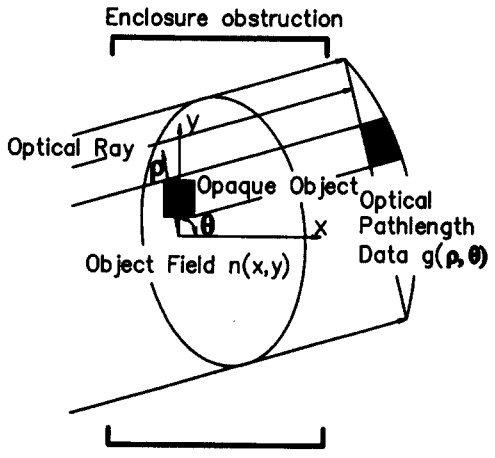

Fig. 1 Optical pathlength data of a flow field in multidirectional interferometery.

In the series expansion method, a field $n(x, y)$ is approximated by a finite expansion of either local or nonlocal basis functions:

$$n(x, y) \cong \sum_{i=1}^{N} c_i b_i(x, y) \tag{2}$$

where $b_i(x, y)$ are the series expansion basis functions and c_i are the corresponding coefficients. In the local basis function approach, the basis (domain of support) of an individual term is confined to a local region in the field. The line integral transform is linear. Therefore, the transform and its inversion can be accomplished on a term-by-term basis. In either of the series expansion methods, local or nonlocal basis functions, the reconstruction needs to determine the coefficients c_i by solving a system of linear algebraic equations:

$$g(\rho_j, \theta_j) \cong \sum_{i=1}^{N} c_i a_i(\rho_j, \theta_j) \tag{3}$$

where $a_i(\rho_j, \theta_j)$ is the line integral transform of $b_i(x, y)$ and subscript j represents measured data points. Various techniques including the least-square method and algebraic reconstruction technique[8] can be employed in solving the equations. The series expansion based on local basis functions is convenient in incorporating a priori information, i.e., boundary shape, positiveness, etc. A typical series expansion method is the fixed grid method.[6] This conventional method (CM) employs square-pulse local basis functions defined in uniform grid

elements. Series expansion methods, enabling direct reconstruction by fitting only available data with an approximate series, are convenient for limited-data reconstruction. In principle, they do not require data interpolation. Under limited-data conditions, however, the linear algebraic equations resulting from conventional approaches become ill behaved because of a uniform basis size employed and thus produce distortions in reconstruction.

In an effort to deal with the ill-posed reconstruction problems, Cha and Cha[11] have developed a new algorithm termed the variable grid method (VGM). The VGM employs nonuniform rectangular-pulse local basis functions, which is similar to assigning a constant value to a grid element in computational fluid dynamics. The VGM employed for this study can be briefly summarized as follows. In this method, the field is divided into rectangular bases of different sizes and aspect ratios so that they could have the following characteristics. First, the bases are adjusted such that an appropriate number of rays pass through each of them. This allows a reasonably uniform degree of redundancy to an individual coefficient in the linear algebraic equations. The resulting well-behaved matrix is believed to yield a stable solution of the coefficients, that is, individual pulse-function values in this case. Second, the algorithm enables the region of interest with more heavily scanned probing rays to contain finer bases and thus to be reconstructed with better accuracy and resolution. In the case when data interpolation is necessary, the interpolation intervals can be proportional to the original data intervals. In this way, the spatial resolution information can be preserved. As a result, the VGM is believed to allow enhanced reconstruction resolution and accuracy by providing a larger number of appropriate series terms under ill-posed conditions and local undersampling. Algorithm of VGM can be found in Ref. 11.

The major objectives of this study are to demonstrate the practical applicability of the HIT and the merits of the VGM over CM through real flow reconstructions of reasonable complexity.

2. Experiment

In this study, a laminar steady natural convection flow around two interacting isothermal cubes in glycerine was investigated experimentally. The heating cubes, whose centers were apart by 1.77 times of a side length along a 45° diagonal line, were placed in a rectangular test section ($25.4 \times 25.4 \times 35.6$ cm^3) with two optical windows (15.2 cm in diameter). The surface temperature of each cube was kept constant by controlling the heater power and was monitored with five thermocouples embedded on each face except for one symmetric side face. The ambient fluid temperature was maintained stable by circulating constant temperature water through the heat exchanger tubing that covered the inside walls of the test section. Eleven thermocouples, two around each cube and nine in the region unaffected by the heating, were inserted to monitor the fluid temperature. In the study, the object field was rotated with respect to a fixed probing beam, as shown in Fig. 2, to acquire multidirectional projection interferograms. This noninstantaneous data acquisition required the flow conditions be reasonably identical from run to run. In practice, multidirectional illumination with diffusers and phase gratings[6] can be employed for instantaneous capture and corresponding reconstruction of flow fields, but only with limited angular scanning. Thus, improved computational tomographic re-

construction is needed for its practical applications.

Throughout the study, the ambient fluid temperature fluctuated less than 0.1℃ between runs, and the cube surface temperatures varied less than 0.03 ℃ at the thermocouple positions. Real-time holographic interferometry confirmed that the test section was large enough to prevent wall effects on the flow around the cubes.

2.1 Holographic interferogram recording

As indicated, a conventional procedure of double-exposure holographic interferometry was adopted to provide data of limited scanning. In the optical setup shown in Fig. 2, an argon-ion laser beam was split into two: one for the plane object beam and the other for the spherical reference beam. Holograms were recorded on 10.2×12.7 ㎠ plates, Agfa-Gevaert 10E75. Both holograms and holographic interferograms were processed by a standard procedure.[6] The fluid in the test section was allowed to reach a quiescent and constant temperature state for several hours, and thus it was expected that the cubes reached thermal equilibrium with the surrounding fluid. The first holographic exposure was then taken and the cubes were energized. After a steady state was attained, the second exposure was made. The recording process was repeated at various projection angles starting from $-40°$ to $40°$ in steps of $10°$ by rotating the cubes.

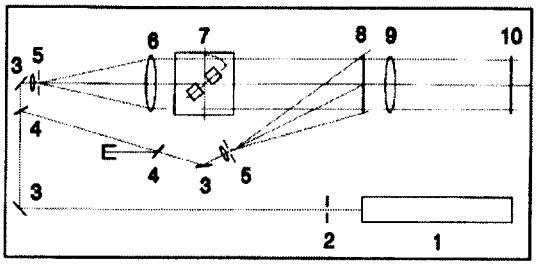

(1) argon-ion laser, (2) shutter, (3) mirror, (4) variable beamsplitter, (5) objective pinhole assembly, (6) collimating lens, (7) test section and rotated model, (8) hologram, (9) imager, and (10) interferogram

Fig. 2 Optical arrangement.

The reconstruction of two object waves, that is, the formation of interferograms, was done with the same setup for hologram recording with the object beam blocked. The holographic interferograms were photographed on film plates and then scanned to extract the OPD with a charge-coupled device (CCD) camera. This approach was adopted since the field was too large to be captured directly by a CCD camera with sufficient resolution. Figure 3 shows two typical holographic interferograms taken at a projection angle of $10°$. Since the supporting bars of the cubes and thermocouples disturbed the adjacent flow field, two interferograms as shown were required to produce a composite single-projection interferogram: one with the supporting bars on the right-hand side (RHS) and the other with them on the left-hand side (LHS).

2.2 Interferogram reduction

In digitization of interferograms by a CCD camera enlarging optics was needed to resolve very fine fringes near the cubes so that at least 10 intensity data could be obtained for each fringe. Several digitized images were thus captured for each interferogram with a precision translation stage and then merged to form a complete set. Phase-shifting techniques can provide accurate interferometric data reduction. However, these techniques are difficult to apply to nondiffuser illumination for large flow measurements with opaque objects as in this experiments. Even when a phase-shifting tech-

nique is applied, it is necessary to subsequently apply regression if heat transfer coefficients, that is, field gradients, are calculated. In regression methods, the gradients can be found directly from the approximating model. For these reasons, a nonlinear regression technique that can provide comparable accuracy except for longer processing time is employed.

In the regression technique, digitized data are fit by equation (4) which represents noiseless fringe patterns:

(a)

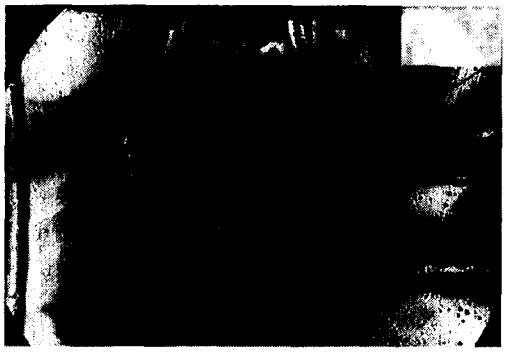

(b)

Fig. 3 Holographic interferograms at a projection angle of 10° : support bars at (a) RHS and (b) LHS.

$$I(\rho) = B(\rho) + A(\rho) \times \cos\{p(\rho)\} \quad (4)$$

where $B(\rho)$, $A(\rho)$, and $p(\rho)$ represent the background intensity, modulation amplitude, and phase functions, respectively. Each of these can be approximated by a polynomial or other function with the unknown parameters to be found. For most cases, second-order polynomials for the background intensity and third-order polynomials for the amplitude modulation and phase functions were employed.

A typical plot of measured intensity is shown in Fig. 4(a). This curve corresponds to a horizontal line of the interferogram of Fig. 3(a), along the left half of section BB in Fig. 5. Figure 4(a) also shows data points from the nonlinear regression analysis, superimposed on the measured intensity. The extracted phase function $p(\rho)$ is shown in Fig. 4(b). The phase functions extracted from each projection angle θ were combined to produce the two-dimensional data sets of $p(\rho_j, \theta_j)$. The OPD $g(\rho_j, \theta_j)$ in equation (3) can then be found by dividing by $2\pi/\lambda$, where λ is the laser wavelength.

2.3 Computational tomographic reconstruction

The refractive index field was reconstructed by both the VGM and CM for close examination of the two horizontal planes at sections AA and BB in Fig. 5 with and without an opaque object, respectively. Since the fields were approximated by step functions in these methods, the reconstructions were smoothed by B-spline interpolation. The center values of the bases were employed for this purpose. Since the field gradients vary substantially, the OPD were unevenly sampled, depending on fringe spacing. In this manner, the spatial information

in the area of interest could be preserved while minimizing the computational burden. The portion of the OPD was not available because of being blocked by an opaque test model and reduced view angle of 80°, thus resulting in severely ill-posed conditions. For sections AA and BB in Fig. 5, the total data points were about 635 and 460, respectively.

The optimum values of input parameters in reconstruction can be approximately found with the sampled OPD through computer simulation of experiments. This strategy is briefly summarized as follows, First, an approximate field is assumed; that is, results from a numerical code in Figs. 6(a) and 7(a) were adopted in the study. Next, OPD are generated from the approximate field through the line integral transformation based on the same experimental conditions. The field is then reconstructed with the computer generated OPD and compared with the original field. For a given data set, the optimum input parameters, including the number of bases, can be found from the best reconstruction. In many applications the field to be reconstructed may not be available from numerical codes. However, even a crude field approximation can reasonably provide optimum parametric values through computer simulation of experiments.

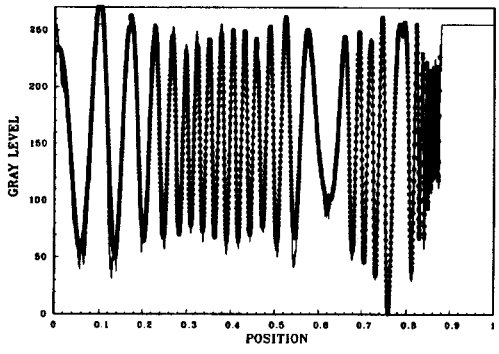

(a)

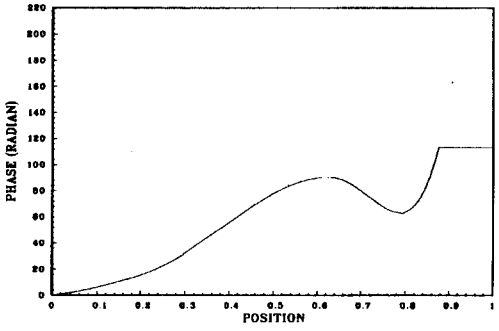

(b)

Fig. 4 Example of interferogram reduction: (a) plot of regression data (dotted line) and measured intensity (solid line) and (b) extracted phase function.

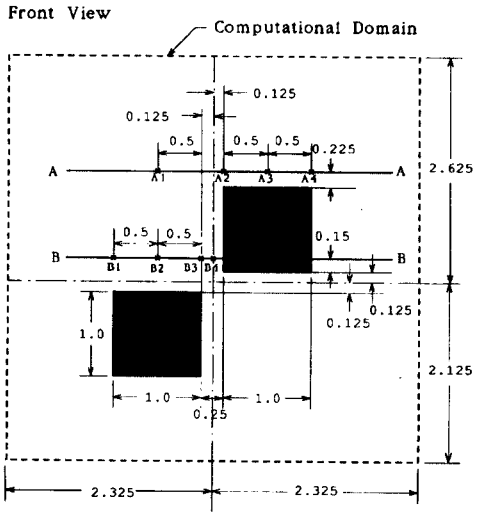

Fig. 5 Vertical symmetric plane of the flow field indicating two horizontal cross sections of investigation and thermocouple positions: dimensions are normalized by a cube side length.

3. Reconstruction Results and Comparison

Refractive index fields were reconstructed by both the VGM and CM with the corresponding optimum numbers and configurations of basis functions found by the computer-simulation procedure as indicated. For the reconstruction of section AA in Fig. 5, a circular boundary constraint was applied; that is, the value was set to zero beyond the boundary. Figures 6(b) and (c) show the reconstructions by both the VGM and CM at a view angle of 80° . When compared with the flow field in Fig. 6(a), the overall shape of the VGM reconstruction is quite similar. For the CM reconstruction, on the other hand, the hump gets distorted. It is also observed that there is multiplied noise component near ambient region due to ill-behaved coefficient matrix.

Similarly to the reconstruction of section AA without an opaque object, the field at section BB in Fig. 5 with an opaque object, as seen, was also reconstructed by both the VGM and CM. An elliptical boundary constraint is applied at this time. Figures 7(b) and (c) show the reconstructions by both the VGM and CM at a view angle of 80° . As seen, the VGM reconstructs the hump above the lower opaque object successfully. However, the CM fails to do so nor the overall shape of the flow field. Because of the ill-posed nature of the reconstruction, the CM requires a relatively small number of basis functions and this might be the reason for the inferior performance. The region close to the opaque object surfaces of constant value, where steep gradients occur, was probed by a very limited number of rays, and it is thus difficult to provide accurate reconstruction even with the VGM. Interpolation based on a priori knowledge of the surface val-

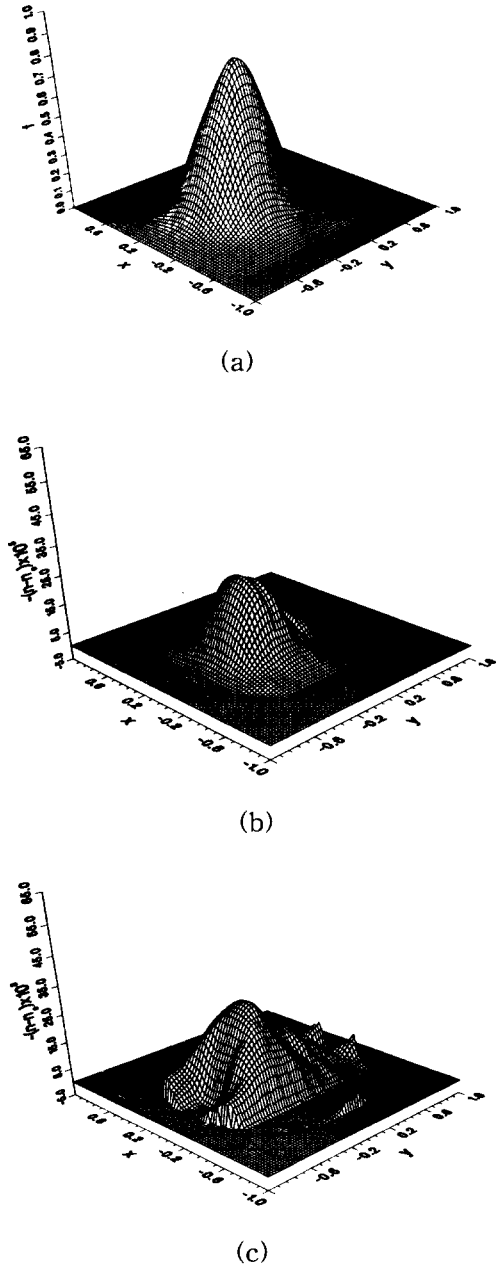

(a) (b) (c)

Fig. 6 Thermal plume at section AA: (a) flow field obtained from numerical solution; (b) reconstruction by the VGM; (c) reconstruction by the CM, at a view angle of 80° .

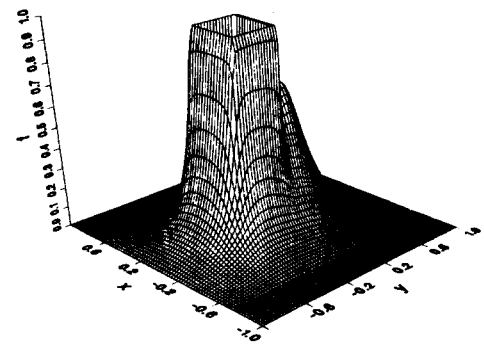

(a)

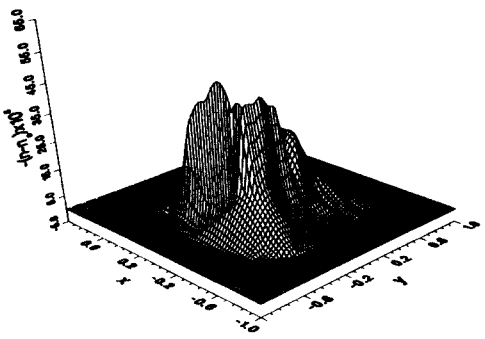

(b)

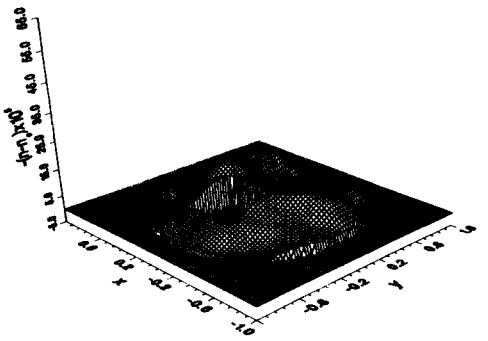

(c)

Fig. 7 Thermal plume at section BB: (a) flow field obtained from numerical solution; (b) reconstruction by the VGM; (c) reconstruction by the CM, at a view angle of 80° .

ue is thus necessary to minimize the reconstruction errors near the opaque objects.

To measure temperature T by interferometry, refractive index n needs to be converted to temperature. For implementation, an empirical equation within an expected uncertainty of less than 2% was adopted:[14]

$$\frac{dn}{dT} = -\frac{3}{2}\frac{n(n^2-1)}{2n^2+1}\beta \tag{5}$$

where β is the volumetric coefficient of thermal expansion of a fluid. For simplicity, equation (5) was further approximated by a linear relationship in the temperature range of interest.

The extent of the ambient fluid at about 22.8℃ was relatively large compared with the thermal plume size. In reconstruction, the ambient temperature was assumed to be uniform. However, its local fluctuations of unknown magnitude, which may increase with average temperature, is believed to be a major source of reconstruction inaccuracy. Other error sources, including the interferogram reduction uncertainty less than $\lambda/100$,[13] for example, may be negligible. To examine the reconstruction reliability, the results from the HIT were compared with those from a 3-D control-volume finite difference code as plotted in Figs. 6(a) and 7(a) and the thermocouple (TC) measurements as indicated in Fig. 5. The temperature measurements were made at four locations in each symmetric center line of the two horizontal planes; that is, A1-A4 for section AA and B1-B4 for section BB after recording the multidirectional holograms. Only four thermocouples for each horizontal plane were inserted in two separate runs to minimize flow disturbance. The flow fields during the TC measurements are believed to replicate the ones during multidirectional hologram recording.

For comparison, the temperature values obtained from the VGM reconstructions of Figs. 6(b) and 7(b) are shown in Table 1 for the individual thermocouple positions. These two reconstructions can represent good interferometric measurements. The temperatures from the TC, HIT, and numerical computation are denoted by T^{TC}, T^{RE}, and T^{N}, respectively in the table. When the relative temperature difference ε is thus defined as the percent of the ambient fluid temperature T_∞ by

$$\varepsilon = 100 \times \frac{(T^i - T^j)}{T_\infty} \quad (6)$$

where $(T^i - T^j)$ is the difference between measurements, the results can be summarized as in Table 2. As expected, the results for section AA are better than those for section BB. Since section BB has substantially greater temperature gradients than section AA, slight mispositioning of its thermocouples may result in appreciable differences.

The refractive index fields reconstructed by the CM, as shown in Figs. 6(c) and 7(c), were also converted into temperature fields. The relative temperature differences of these VGM and CM reconstructions from the TC measurements are listed in Table 3. The temperature measurements at A3 and B2 show maximum values among those at four locations of each section. The examination at the two points indicates that the reconstruction values are always less than the TC measurements and their absolute errors become in general larger than those at other points. This implies that the field humps of maximum value become lower. For section AA in Table 3, ε values of the VGM are not greatly lower than those of the CM. However, appreciable differences in overall reconstruction artifacts can be noticed

Table 1 Temperatures obtained from TC, HIT, and numerical computation

TC No.	T^{TC}, °C	T^{RE}, ℃	T^{NU}, °C
A1	23.75±0.01	23.7	23.46
A2	24.69±0.01	24.1	24.97
A3	25.34±0.01	24.6	25.19
A4	23.93±0.01	24.0	24.26
B1	23.42±0.01	23.7	23.55
B2	25.07±0.01	24.5	24.50
B3	24.22±0.01	24.2	24.80
B4	24.67±0.01	24.2	24.89

Table 2 Relative temperature difference between the results from TC, HIT, and numerical computation

TC No.	ε, %		
	$T^{RE} - T^{TC}$,	$T^{NU} - T^{TC}$	$T^{NU} - T^{RE}$
A1	-0.35	-1.28	-0.77
A2	-2.12	1.23	-0.66
A3	-2.69	0.62	2.13
A4	0.13	1.43	1.12
B1	0.95	0.58	-0.43
B2	-2.37	-2.49	-0.15
B3	-0.24	2.58	2.51
B4	-1.89	0.98	2.75

Table 3 Relative temperature differences of reconstructions at a view angle of 80°

TC No.	ε, %	
	VGM	CM
A1	-0.35	0.88
A2	-2.12	-1.26
A3	-2.69	-2.36
A4	0.13	-0.32
B1	0.95	0.00
B2	-2.37	-5.44
B3	-0.24	-1.47
B4	-1.89	-3.07

in Figs. 6(b) and (c), which demonstrate the superior VGM reconstruction. For section BB, the VGM difference is fairly stable whereas the CM difference shows a much larger value. This trend can also be confirmed by the reconstructed plots by the VGM and CM in Figs. 7(b) and (c).

This study of limited data reconstruction indicates that the VGM outperforms the CM, especially for those with an opaque object. The HIT reconstruction with the VGM can provide a reasonable accuracy for a view angle of 80° for the test field.

4. Conclusion

The HIT reconstruction results with limited interferometric data agree well with the numerical computation and TC measurements. Its uncertainty is believed to be close to the ambient fluid disturbance that is not known. The HIT can thus be appropriate for thermal-fluid experiments that often produce severely limited data. Even though a traditional approach for the parametric study by rotating the test field for multidirectional scanning is employed in this study, in real applications, the HIT can utilize diffuser or grating illumination to capture an instantaneous flow field. The modification is straightforward.

Acknowledgment

This work was supported in part by grant No. 1999-2-304-001-3 from the Basic Research Program of the Korea Science and Engineering Foundation.

References

(1) Doerr, S., 1992, "Measurement of a Three-Dimensional Hypersonic Density Field," AIAA Paper 92-0383.

(2) Snyder, R. and Hesselink, L., 1984, "Optical Tomography for Flow Visualization of the Density Field around a Revolving Helicopter Rotor Blade," Applied Optics, Vol. 23, No. 20, pp. 3650-3656.

(3) Sweeny, D. W. and Vest, C. M., 1974, "Measurement of Three-Dimensional Temperature Fields above Heated Sources by Holographic Interferometry," International Journal of Heat and Mass Transfer, Vol. 17, No. 12, pp. 1443-1454.

(4) Cha, D. J. and Cha, S. S., 1995, "Three Dimensional Natural Convection Flow around Two Interacting Isothermal Cubes," International Journal of Heat and Mass Transfer, Vol. 38, No. 13, pp. 2343-2352.

(5) Hertz, H. M., 1987, "Experimental De-termination of Two-Dimensional Temperature Fields by Holographic Interferometry," Optical Communications, Vol. 54, pp. 131-136.

(6) Vest, C. M., 1979, Holographic Interferometry, Wiley, New York, Chap. 6.

(7) Lewitt, R. M., 1983, "Reconstruction Algorithms: Transform Methods," Proceedings of the IEEE, Vol. 71, No. 3, pp. 390-408.

(8) Censor, Y., 1983, "Finite Series-Expansion Reconstruction Methods," Proceedings of the IEEE, Vol. 71, No. 3, pp. 409-419.

(9) Crowther, R. A., DeRosier, D. J., and Klug, A., 1970, "The Reconstruction of a Three-Dimensional Structure from Projections and Its Applications to Electron Microscopy," Proceedings of the Royal Society of London, Series A: Mathematical and Physical Sciences, Vol. 317, No. 1530, pp. 319-340.

(10) Ramachandran, G. N. and Lakshiminaraya-

nan, A. V., 1971, "Three-Dimensional Reconstruction from Radiographs and Electron Micrographs: Part III-Description and Application of the Convolution Method," Indian Journal of Pure and Applied Physics, Vol. 9, No. 11, pp. 997-1003.

(11) Cha, D. J. and Cha, S. S., 1997, "Variable Grid Decomposition for Ill-posed Interferometric Tomography: Comparison of Algorithms," Optics and Lasers in Engineering, Vol. 28, No. 3, pp. 181-197.

(12) Cha, S. S., 1992, "Holographic Interferometric Tomography for Reconstructing Flow Fields: A Review," AIAA Paper 92-3934.

(13) Slepika, J. S. and Cha, S. S., 1995, "Stabilized Nonlinear Regression for Interferogram Analysis," Applied Optics, Vol. 34, No. 23, pp. 5039-5044.

(14) Murphy, C. G. and Alpert, S. S., 1971, "Dependence of Refractive Index Temperature Coefficients on the Thermal Expansivity of Liquids," American Journal of Physics, Vol. 39, pp. 834-836.